Simulations of classical three-body thermalization in one dimension

M. Eltohfa,* Xinghan Wang, Colton M. Griffin, and F. Robicheaux†
Department of Physics and Astronomy, Purdue University, West Lafayette, Indiana 47906, USA

(Received 29 February 2024; revised 16 May 2024; accepted 3 June 2024; published 8 July 2024)

One-dimensional systems, such as nanowires or electrons moving along strong magnetic field lines, have peculiar thermalization physics. The binary collision of pointlike particles, typically the dominant process for reaching thermal equilibrium in higher-dimensional systems, cannot thermalize a 1D system. We study how dilute classical 1D gases thermalize through three-body collisions. We consider a system of identical classical point particles with pairwise repulsive inverse power-law potential $V_{ij} \propto 1/|x_i - x_j|^n$ or the pairwise Lennard-Jones potential. Using Monte Carlo methods, we compute a collision kernel and use it in the Boltzmann equation to evolve a perturbed thermal state with temperature T toward equilibrium. We explain the shape of the kernel and its dependence on the system parameters. Additionally, we implement molecular dynamics simulations of a many-body gas and show agreement with the Boltzmann evolution in the low-density limit. For the inverse power-law potential, the rate of thermalization is proportional to $\rho^2 T^{\frac{1}{2}-\frac{1}{n}}$, where ρ is the number density. The corresponding proportionality constant decreases with increasing n.

DOI: 10.1103/PhysRevE.110.014114

I. INTRODUCTION

A. Technological motivation

With the advance of technology, very thin systems can be produced that can be approximated as one-dimensional (1D). Examples of 1D gases include quantum-wires made of GaAs [1] or carbon nanotubes [2]. Other examples come from plasma physics where electrons are confined to move along strong magnetic field lines [3], or isolated, far-from-equilibrium, Bose gases [4]. Thus, the properties of 1D systems are of some interest.

One-dimensional confinement considerably affects system properties, such as thermalization process [5], enhanced correlations and collective behavior [6], and anomalous transport and diffusion [7]. In the present work, we study the rate of thermalization of certain 1D systems. This rate measures how fast the equilibrium state is reached if the system starts from a nonequilibrium state. From another perspective, it measures how fast the system loses memory of its initial state.

Unique features of 1D thermalization have been demonstrated. Optical measurements have shown that carrier relaxation is much slower in quantum wires than in bulk and two-dimensional forms [8]. Additionally, molecular dynamical (MD) simulations of a 1D line of electrons have shown the system thermalizes in the order of 10 ns [5], which is a relatively slow rate. However, the dynamics of thermalization of quasi-1D systems, consisting of nearly decoupled chains, was shown to exhibit nonexponential approach to equilibrium [9].

For this paper, we simulate the interaction of classical pointlike particles that are confined to move in 1D. We define the thermalization rate by how fast a special velocity of a particle irreversibly diffuses into the distribution of the rest of the system. With this definition, we show that the 1D gases under study exhibit very slow thermalization rates.

B. Theoretical motivation

1. Two-body thermalization

In the kinetic theory of 3D gases, thermalization through binary collisions has been thoroughly studied [10]. Binary collisions are the dominant interaction if the gas is dilute; many-particle collisions are suppressed by powers of the density [11]. Although a binary collision is tightly constrained by several conservation conditions, there is freedom for the particles to change their directions based on their impact parameter.

In the center of mass frame of the two colliding bodies, the equations of motion can be integrated and a nonzero differential cross-section can be obtained. Subsequently, the cross-section determines the rate of scattering from and into a tiny volume in coordinate-velocity space of the one-particle distribution. These rates can be used in the Boltzmann equation to propagate the distribution [10]. By Boltzmann's H theorem, a nonzero cross-section guarantees the thermalization of the system to equilibrium. Binary collisions also lead to thermalization in 2D although the details are different.

Thermalization through binary collisions, however, does not work in a 1D gas of identical pointlike particles. Consider two particles of mass m elastically colliding with incoming velocities v_1, v_2, and outgoing velocities w_1 and w_2. Conservation of energy and momentum must hold. This, in 1D, entails two equations which completely determine that $w_2 = v_1$ and $w_1 = v_2$. This is a trivial swapping that leads to the same velocities and, therefore, to an unchanged velocity distribution [5].

*Contact author: meltohfa@purdue.edu
†Contact author: robichf@purdue.edu

The triviality of the binary collision in 1D hinges on two assumptions [5]: (1) The dispersion relation is parabolic which is well established; (2) there is no exchange of momentum with the substrate (the crystal or the medium the particles live in). The latter assumption works well in regimes of energy less than 1 eV for crystal spacing 10^{-10} m, or if the particles live in 1D vacuum. In this work, we assume that the particles are constrained to move on a ring or a line with no external forces.

2. Many-body thermalization in 1D

It was shown in Ref. [5] that many-body Coulomb scattering can thermalize a one-dimensional electron gas in a single-subband GaAs quantum wires. This was done through classical molecular dynamics (MD) simulations. In the study, the gas is dense enough such that the mean potential energy is of the order of the mean kinetic energy ∼100 K ∼ 10 meV. It was calculated that the relaxation time is of order 10 ns and increases rapidly for lower densities.

3. Three-body thermalization in 1D

Since binary collisions cannot thermalize a 1D system, we study thermalization through the next simplest process, the three-body (ternary) collisions. In very dilute gases, which is our main focus, the ternary collision is dominant over the higher order collisions. The ternary collision is generally nontrivial and can generate new velocity states. For long-range interacting homogeneous 1D systems, it was shown that they can thermalize through three-body effects, but their relaxation is drastically slowed down [12]. The three-body problem, however, is nonintegrable [13] (except in very special cases [14]), so we study its trajectories numerically.

Three-body thermalization has also been addressed in Ref. [15] for a model problem. The scattering rate from a triple of initial momenta to a triple final momenta was assumed for simplicity to be constant as long as the incoming momenta and the outgoing momenta satisfy energy and momentum conservation. In such cases, the Boltzmann Eq. (B1) is exactly solvable. This constant scattering rate, however, was not derived from an interparticle potential energy. Additionally, it was found that the rate of collisions, and hence the rate of thermalization, goes as ρ^2 but is not affected by temperature or the average kinetic energy. With the rates computed from an interparticle potential, we will show that if we start from a quasithermal distribution of temperature T, the rate of thermalization depends not only on ρ but also on T.

C. Goal and plan

In the present paper, we first introduce a model of a 1D gas on a ring and a model of thermalization. We consider a system with pairwise inverse power potential with power $n \geqslant 2$. This potential is formally long-range, since any particle can affect any other particle with nonzero force. But for low densities and high temperatures, which we assume, this force is small enough that long-range effects can largely be ignored [16]. We consider the evolution of a "δ-perturbed" thermal state. Previous studies [5,9] considered the evolution of a bimodal distribution or a modified Gaussian [16].

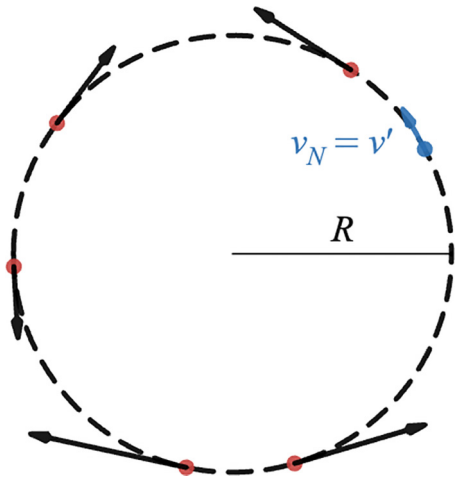

FIG. 1. Particles on a ring of radius R. All but one particle are initialized from a thermal distribution. The "special" particle (in blue) is initialized with a special velocity v'. The special particle represents a perturbation to the thermal state.

Second, we implement MD simulations and discuss the scaling of the thermalization rate, which we define as the initial rate of the spread of the perturbation. Third, using Monte Carlo simulations, we calculate a three-body collision kernel for the inverse power potential and the Lennard-Jones potential. Using the kernel information, we show how the transition rates scale with ρ and T and compute the thermalization rate for a range of parameters. Fourth, the collision kernel is used in the Boltzmann equation to evolve the perturbation and this method is shown to be in agreement with the MD simulations. Finally, we discuss the shape of the kernel and how it changes with the inverse potential power n.

II. GAS AND THERMALIZATION MODEL

We consider N identical particles of mass m constrained to move on a ring of radius R as in Fig. 1 with pairwise repulsive inverse power-law potential

$$U(d) = \epsilon\left(\frac{l_0}{d}\right)^n, \tag{1}$$

where d is the pairwise separation (the 2D distance in the plane of the ring), l_0 is the basic unit of length at which the potential energy is equal to some interaction strength $\epsilon > 0$, and n is an even integer $\geqslant 2$.

The locations of the particles are parameterized by the angles ϕ_i and the 2D distance (the length of the chord) between particles i and j is

$$d_{ij} = 2R\,\sin\left(\frac{|\phi_i - \phi_j|}{2}\right). \tag{2}$$

The energy of the system is

$$E = \sum_{i=1}^{N} \frac{mR^2\omega_i^2}{2} + \epsilon\left(\frac{l_0}{2R}\right)^n \sum_{i,j>i}^{N}\left[\sin\left(\frac{\phi_i - \phi_j}{2}\right)\right]^{-n}, \tag{3}$$

where ω_i is the angular velocity of particle i.

We choose a ring to represent the 1D system instead of a line so that particles do not escape to infinity under repulsive forces. Modeling a line would require a confining potential which leads to the particles at the edges experiencing a different environment from those in the center of the range. Although the aim of the paper is studying the gas in 1D, we use the 2D distance along the chord in Eq. (2) instead of the 1D distance along the arc so that the torque would be continuous in ϕ and would be 0 for particles on opposite sides of the ring. It also has the added benefit of smoothly cutting off the interaction between two particles as $|\phi_i - \phi_j|$ increases. This introduces curvature effects which distort from a true 1D system. However, these effects become negligible at large R. The choice of a finite ring with periodic boundary also introduces finite size effects that diminish at large R and N. To simulate a particular linear number density, $\rho = N/R$, we decrease the ring effects by doubling R and N until our results converge.

We consider a thermal initial condition sampled from a Boltzmann distribution with temperature T. In particular, the initial velocity $v(t=0) = R\,\omega(t=0)$ of a particle follows the Maxwell-Boltzmann statistics with probability density function:

$$f_0(v) = \frac{1}{\sqrt{2\pi\, v_{\rm th}^2}} e^{-v^2/2v_{\rm th}^2}, \tag{4}$$

where $v_{\rm th} = \sqrt{kT/m}$ is the velocity scale set by the temperature. k is the Boltzmann constant. The initial locations are chosen randomly according to a relative potential energy Boltzmann factor $\exp(-{\rm PE}/kT)$, where PE is the total potential energy [second term in Eq. (3)]. In this way, a configuration with a very close group of particles occurs rarely and, therefore, rejected with a high probability in our simulations. Also, the number density ρ is homogeneous on average. In our MD simulations, we ensure uniform density by averaging the results over many runs with different initial conditions. We do not consider effects of density variations along the ring (which lead to the diffusion of the particles) in this paper. However, we will show how the relaxation rate depends on the overall density.

In this work, we assume high enough T and small enough number density, ρ, so that the average kinetic energy is much greater than the potential energy (unlike in Ref. [5], where the energies are comparable). In this regime, correlations between positions of the particles can be ignored. At the other extreme of low T and high ρ, position correlations become important because the system condenses to a solid with periodic arrangement of particles.

We consider a perturbation to the thermal state by forcing one of the particles (e.g., the Nth particle) to start at a particular velocity v' as in Fig. 1. While all the rest of the phase variables obey the thermal distribution statistics, this particle's velocity will disobey the Maxwell Boltzmann distribution in Eq. (4) and will rather have a δ-function distribution centered at v'. We refer to such a particle as the "special" particle and its velocity as the "special velocity," while we refer to the rest of the particles as "thermal." The velocity probability density function of the total system is

$$f(v, t=0) = \frac{N-1}{N} f_0(v) + \frac{1}{N} h(v, t=0), \tag{5}$$

where $h(v,t)$ is the normalized perturbation (integral over v is 1) such that

$$h(v, t=0) = \delta(v - v'). \tag{6}$$

If we introduce the scaled velocity $u = v/v_{\rm th}$, then the normalized (integral over u is 1) initial distribution is

$$f(u, t=0) = \frac{N-1}{N} \frac{1}{\sqrt{2\pi}} e^{\frac{-u^2}{2}} + \frac{1}{N}\delta(u - u'). \tag{7}$$

Our goal is to study the evolution of h. According to the Boltzmann H-theorem [10], the steady state distribution $f(v,\infty)$, and therefore $h(v,\infty)$, is the equilibrium distribution f_0. This is strictly true in the thermodynamic limit $N \to \infty$. For finite N, however, the steady state has a slightly different temperature $T_f \simeq (N - 1 + u'^2)T/N \approx T$ for large N, which is a result of energy conservation.

To investigate the rate of thermalization, we introduce Γ to be the initial rate of change of the variance of the perturbation:

$$\Gamma = \left.\frac{d\langle (u-u')^2\rangle_h}{dt}\right|_{t=0}. \tag{8}$$

This definition of Γ implies that if the perturbation continues spreading at the initial rate, then it takes time of order $1/\Gamma$ for the perturbation $h(u)$ to reach variance $\sim$1, i.e., the special particle reaching the temperature of the bath. This definition is introduced to enable the quantification of the notion of the thermalization rate.

We choose this particular type of perturbation because it is easy to track and characterize during the simulations. The initial perturbed distribution is a Gaussian with a large narrow spike at v'. When the number of particles is large, the Gaussian background is mostly unaffected during the evolution. However, during the early stages of the thermalization the spike spreads out but remains significantly higher than the background Gaussian. It is therefore possible, during early times, to track the evolved perturbation by only tracking a small range of velocities (we choose a range of $0.2v_{\rm th}$ centered around v') and subtracting the background to get h. This eliminates the need to make a histogram of all the velocities and makes it possible to get a clearer evolution of the perturbation. Although our choice is mostly for ease of computations, it will be shown below that the relaxation rate, Γ, is only different by a small numerical factor for different types perturbations.

We run many MD simulations (as described in detail in Appendix A) where the $N-1$ thermal particles are randomly chosen from a thermal distribution. Averaging over these many runs gives an average $h(u,t)$. From our simulations, the average $h(u,t)$ starting from $\delta(u)$ is shown for two times in Fig. 2. As expected, the perturbation's peak height decreases and its width increases as the system evolves. The times shown are early in the thermalization process where the population only spreads to small velocities ($|u| < 0.06$). However, the cusp feature of the δ function is maintained throughout this time period, which is an indication that the gas is far from equilibrium. The parameters of the simulated

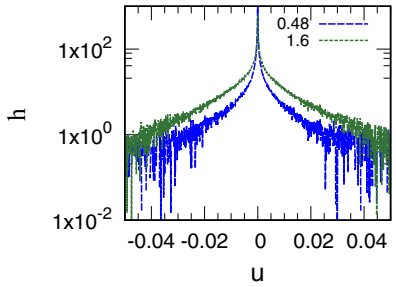

FIG. 2. MD simulated evolution of the probability distribution of the perturbation $h(v,t)$ which is initially localized at $v=0$. The two times shown are 0.48 and 1.6 ($\times 10^{-4}/\Gamma$) which are very early in the thermalization process. The x axis is the scaled velocity $u = v/v_{\rm th}$. Comparing the distribution at these two time instants and at $t=0$ (a δ function of u), the perturbation width increases with time as its height drops. The fluctuations at the edges of the curves are due to statistical noise.

gas are $l_0 = 1\,\mu$m, $\epsilon = 1\,$eV, $kT = 100\,$meV, $m = m_e$ (mass of the electron), $n = 6$, $N = 41$, and $R = 6400\,\mu$m. The times shown are $t_f = 960, 3200\,$ns $= 0.48, 1.6 \times 10^{-4}/\Gamma$, where Γ is computed in Eq. (23).

In the rest of the paper, we show how Γ depends on the system parameters $\{R, N, m, T, l_0, \epsilon, n, u'\}$. To extract this dependence, we do MD simulations for different parameter sets; however, as argued in Appendix A, such N-body simulations are computationally very expensive when N is large or the propagation time, t_f, is large.

III. BOLTZMANN EVOLUTION OF THE GAS

A more efficient method to study Γ is to consider the simpler process by which our system thermalizes, the ternary collision. By knowing the frequency of such collisions and how they change the particle velocities, we can propagate the velocity distribution in time. The recipe of such method is the Boltzmann equation. For those reasons, we choose to focus on the Boltzmann method and limit ourselves to a few MD simulations. In particular, we use the MD simulations to extract some preliminary scaling for Γ and as a benchmark to verify our Boltzmann calculations.

The Boltzmann evolution is an example of a continuous time Markov chain in which the next step distribution is only dependent on the current distribution. If the perturbation is initially localized at v', $h(v,0) = \delta(v - v')$, then after infinitesimal duration dt, the perturbation becomes

$$h(v, dt) = \delta(v - v') + dt K_{v' \to v}, \tag{9}$$

where the kernel $K_{v' \to v}$ is the rate of transitioning from velocity v' to the range between $v - \frac{\Delta v}{2}$ and $v + \frac{\Delta v}{2}$ per Δv in the limit $\Delta v \to 0$. After a finite time, the perturbation delocalizes to a continuous range of v; the evolution equation then becomes

$$h(v, t + dt) = h(v,t) + dt \int_{-\infty}^{\infty} K_{v' \to v} h(v', t)\, dv'. \tag{10}$$

Numerically, we work with a discretized version of the distribution and the kernel. The velocity axis is divided into bins of width Δv, which we choose as a fraction of $v_{\rm th}$. Each bin is labeled by its center velocity $v_i = i\Delta v$ and extends from $v_i - \frac{\Delta v}{2}$ to $v_i + \frac{\Delta v}{2}$. Equation (10) becomes

$$h_i(t + dt) \approx h_i(t) + dt \sum_{j=-\infty, j\neq i}^{j=\infty} \Delta v \left[K_{v_j \to v_i} h_j(t) - K_{v_i \to v_j} h_i(t) \right], \tag{11}$$

where $h_i \Delta v$ is the population in bin v_i. The positive term in the square brackets represents the flow of population to bin v_i from all other bins, while the negative term represents the flow out of bin v_i to all other bins.

A. Monte Carlo simulation of K

To calculate the transition rates $K_{v' \to v}$, we focus on the special particle with velocity v' and treat the rest of the system as a thermal bath of temperature T and number density ρ. Through a Monte Carlo (MC) simulation on a line [17], we simulate the possible collisions the special particle (referred to as particle 1) encounters with two other thermal particles (referred to as particles 2 and 3).

The set of all possible three-body collisions can be determined by first changing to an inertial frame moving with velocity v' where the special particle is at rest before the collision. In this frame, particle 1 is initialized with velocity $v_1 = 0$ at the origin $x = 0$. We consider an observation region of length L centered around the special particle. In a small time duration, there is a probability that a thermal particle (particle 2 or 3) will enter the observation region from either side at $x = \pm L/2$ with some velocity (v_2 or v_3). We model the 'launching' of the particles into the observation region as a Poisson process with rate r. The rate r determines the distribution for the delay Δt between the launched particles. By studying the phase space distribution of a particle in the considered thermal bath, we determine r and the statistics of the launched particles. These statistics and the steps of the algorithm are described in Appendix C.

This idea of tracking a particle in contact with a bath in thermal equilibrium is similar to the analysis of Brownian motion [18]. But instead of following the position of a tagged particle to see how it diffuses in space (like in a random walk), we track the special velocity and see how it changes due to three-body collisions. By studying the velocity fluctuations and their rates, we can infer the relaxation rates of macroscopic perturbations. This is similar to using the time correlation function of a particle velocity in Brownian motion to calculate the diffusion coefficient [18]. Deducing the thermalization rate from the velocity changes is an application to the Onsager regression hypothesis which relates macroscopic nonequilibrium disturbances to microscopic fluctuations in the corresponding equilibrium system [19].

IV. RESULTS

A. Scaling behavior of the N-body gas

In this section, we extract the three-body scaling using MD simulations. Before presenting the results of the simulations, we predict the scaling by analyzing the equations of motion of

the N-body gas on the ring. The equations of motion follow from the energy in Eq. (3):

$$mR\frac{d\omega_i}{dt} = \sum_{j\neq i}^{N} \frac{n\epsilon}{2} \frac{\left(\frac{l_0}{2R}\right)^n}{R\left[\sin\left(\frac{\phi_i-\phi_j}{2}\right)\right]^{n+1}} \cos\left(\frac{\phi_i-\phi_j}{2}\right),$$
$$\frac{d\phi_i}{dt} = \omega_i. \tag{12}$$

These equations can be scaled resulting in equations of motion independent of all dimensional parameters.

We reduce the number of parameters by first identifying the length, time, and angular velocity scales. The angular velocity scale comes naturally from the thermal velocity: $\omega_{\rm th} = v_{\rm th}/R$, where $v_{\rm th}$ was defined in the context of Eq. (4). The dynamical timescale is proportional to the average orbital time: $t_d = 1/\omega_{\rm th}$. The simple form of the inverse power potential is utilized to find the length scale. The pairwise interaction can be rewritten as

$$U(d) = kT\left(\frac{l}{d}\right)^n, \tag{13}$$

where

$$l = l_0\left(\frac{\epsilon}{kT}\right)^{\frac{1}{n}} \tag{14}$$

is the length scale (closest approach distance) set by the temperature.

If the scaled angular velocity is $\tilde{\omega} = \omega/\omega_{\rm th}$ and the scaled time is $\tilde{t} = t/t_d$ then

$$\frac{d\tilde{\omega}_i}{d\tilde{t}} = \sum_{j\neq i}^{N} \frac{n}{2} \frac{c}{\left[\sin\left(\frac{\phi_i-\phi_j}{2}\right)\right]^{n+1}} \cos\left(\frac{\phi_i-\phi_j}{2}\right),$$
$$\frac{d\phi_i}{d\tilde{t}} = \tilde{\omega}_i, \tag{15}$$

where

$$c = \left(\frac{l}{2R}\right)^n. \tag{16}$$

The dynamics of two systems in terms of the scaled variables is identical if their corresponding c, n, and N parameters are the same. The disappearance of the energy scales (kT or ϵ) in the scaled Eq. (15) is owed to the scale invariance of the inverse power potential. In Sec. IV F, we demonstrate how the energies re-enter the dynamics if we consider other potentials such as the Lennard-Jones potential, which does not lead to scaled equations of motion.

From the definition of l in Eq. (14), kT scales as l^{-n}. Furthermore, the density ρ of the particles for a given N scales as R^{-1}. Thus, c scales as $T^{-1}\rho^n$. If one scales $\rho \to a\rho$ and $T \to a^n T$, c remains the same. Therefore, the scaled dynamics [Eq. (15) alongside the scaled initial conditions] remains the same. Given this constraint, one can show that any time unit of the form $\rho^{-s}T^{-(\frac{1}{2}-\frac{s-1}{n})}$ would be invariant under our scaling symmetry. An invariant rate unit γ is thus governed by terms of the form (rewritten using l and $v_{\rm th}$)

$$\gamma \sim \rho^s l^{s-1} v_{\rm th}. \tag{17}$$

Physically relevant timescales could be identified with integer values of $s \geqslant 0$. $s = 0$ gives a timescale $t_c = l/v_{\rm th}$ which is proportional to the interaction time *during* a binary collision. $s = 1$ gives the dynamical timescale t_d which is proportional to the mean time *between* binary collisions. Similarly, $s = 2$ gives the rate of ternary interactions. The probability that two particles existing in an interaction region of length l scales as ρl, and the rate of a third particle entering this region to interact with the other two particles is $\rho v_{\rm th}$. Thus the ternary interaction rate scales as $\rho^2 l v_{\rm th}$.

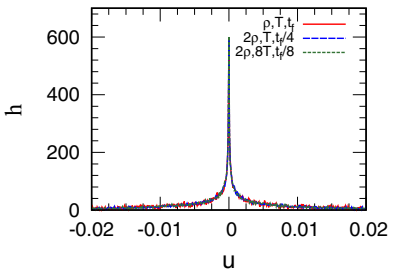

FIG. 3. Three different parameter sets with respective $t_f \propto 1/(\rho^2 T^{1/3})$ give identical final distributions.

For each additional particle colliding, there is one more factor of ρl. For small densities where $\rho l \ll 1$, the relevant term for thermalization is the three-body interaction term since the two body collision is trivial. In the thermodynamic limit $N \to \infty$, we get the scaling of the three-body thermalization rate in Eq. (8):

$$\Gamma = a_n \rho^2 l v_{\rm th}, \tag{18}$$

where a_n is a dimensionless quantity depending only on n in Eq. (1).

From Eq. (18), we expect that the evolution rate is proportional to $\rho^2 T^{1/3}$ for $n = 6$. To test this scaling, we compare a gas with density ρ and temperature T evolving for time t_f with two other cases: 2ρ, T evolving for $t_f/4$ and 2ρ, $8T$ evolving for $t_f/8$. Figure 3 shows the evolved distribution in the three cases. All three curves are the same within statistical uncertainty, which confirms the predicted scaling.

Parameters used in the MD simulation are $N = 161$ particles for three cases: $R = 51\,200\,\mu$m, $kT = 100$ meV, $t_f = 12\,800$ ns; $R = 25\,600\,\mu$m, $kT = 100$ meV, $t_f = 3200$ ns; and $R = 25\,600\,\mu$m, $kT = 800$ meV, $t_f = 1600$ ns. In all cases, $l_0 = 1\,\mu$m, $\epsilon = 1$ eV, $m = m_e$, and $n = 6$. In all cases, the final time $t_f = 1.6 \times 10^{-4}/\Gamma$ as computed from Eq. (18).

B. Scaling of the collision kernel K

A necessary condition for Eq. (10) to reproduce the MD evolution is that $K\Delta v$ as computed from the MC simulations must have the scaling of Γ in Eq. (18). We show that K indeed has the desired scaling under the assumption that $\rho l \ll 1$, where l is defined in Eq. (14). If we define $\tilde{x} = x/l$, $u = v/v_{\rm th}$, and $\tilde{t} = t v_{\rm th}/l$, then those equations are

$$\frac{du_i}{d\tilde{t}} = \sum_{j=0,j\neq i}^{2} \frac{n}{(\tilde{x}_i - \tilde{x}_j)^{n+1}}, \tag{19}$$
$$\frac{d\tilde{x}_i}{d\tilde{t}} = u_i. \tag{20}$$

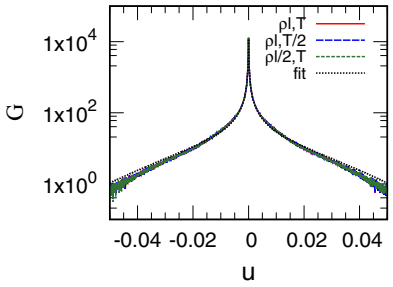

FIG. 4. The dimensionless scaled collision kernel $G_{0\to u}$ for different values of T and ρl. The height and shape of all curves are identical which demonstrates the universal scaling. A fitting function $\frac{\alpha}{|u|^\beta}e^{-u^2/2\sigma^2}$ is also plotted and explained in Sec. IV E.

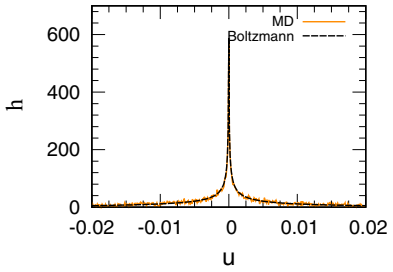

FIG. 5. MD and Boltzmann evolved distributions are in agreement. See text for relevant simulation parameters.

Since the length scale is l, we set the length of the region L to scale with l. In our calculations, for example, we get converging results for the scaling of K at $L = 90l$ and $\rho l = 5 \times 10^{-5}$. The scaled dynamics [Eq. (19)] of a single trajectory only depends on n; that is, scaled initial velocities and positions map to scaled final velocities and positions irrespective of ρ and T. If ρ or T changes, the rate r of launching changes according to Eq. (C1), and the average time spent in the observation region scales as $l/v_{\rm th}$.

Not all simulated trajectories result in a nontrivial change in velocities. Only trajectories where the two launched particles coincide for some time in the region result in effective three-body scattering. Otherwise, the collision is just a sequence of binary collisions that only swap velocities just like in a Newton's cradle.

This coincidence rate $\Gamma_{\rm coin}$ is calculated according to a Poisson process with rate r and observation time window $t_{\rm ob} \propto l/v_{\rm th}$.

$$\Gamma_{\rm coin} = \frac{\text{probability of two arrivals}}{t_{\rm ob}} = \frac{(rt_{\rm ob})^2\, e^{-rt_{\rm ob}}}{2t_{\rm ob}} \approx \frac{1}{2} r^2 t_{\rm ob} \propto \rho^2 v_{\rm th} l \tag{21}$$

The coincidence rate (rate of effective three-body collisions) is proportional to the rate of thermalization, Γ, in Eq. (18) and the kernel $K\Delta v$, which we verify by introducing the dimensionless scaled kernel

$$G_{u'\to u}\Delta u = \frac{K_{v'\to v}\Delta v}{\rho^2 l v_{\rm th}}, \tag{22}$$

where $u = v/v_{\rm th}$. We show in Fig. 4 that G is independent of T and ρ given that $\rho l \ll 1$, $L/l \gg 1$. The scaled kernel $G_{0\to u}$ (denoted by G in the y-axis label) is plotted against the scaled velocity $u = v/v_{\rm th}$. The parameters used in the MC simulations are $v' = 0$ (initially stationary special particle), $n = 6$, $kT = 100\,\text{meV}$, $l_0 = 1\,\mu\text{m}$, $\epsilon = 1\,\text{eV}$, $m = m_e$, bin width $\Delta v = 0.1 v_{\rm th}/2000$, $\rho l = 5 \times 10^{-5}$, and $L = 90l$, where l is defined in Eq. (14).

Since G is independent of ρ and T, the kernel scales like $K\Delta v \propto \rho^2 l v_{\rm th}$. Although we do not explicitly show the scaling with the other parameters (m, ϵ, l_0), it is implied in the definition of l and $v_{\rm th}$ as described in the scaling argument. The scaling of the kernel K with most of the system parameters $\{m, \epsilon, l_0, T, \rho\}$ means that effectively we only need to simulate one representative case for different values of the remaining parameters $\{u', n\}$ to cover the whole parameter space. We implement this idea in a later section.

Using the generated values for G in Fig. 4, the rate Γ in Eq. (18) can be computed using Eqs. (11) and (22) as the rate of change of the variance of h:

$$\begin{aligned}\Gamma &= \left.\frac{d\langle (u-u')^2\rangle_h}{dt}\right|_{t=0} \\ &= \rho^2 l v_{\rm th} \sum_{j=-\infty}^{j=\infty} G_{u'\to u_j}(u_j - u')^2\,\Delta u \\ &= a_n \rho^2 l v_{\rm th},\end{aligned} \tag{23}$$

so the proportionality constant a_n is given by the variance of G:

$$a_n = \langle (u-u')^2\rangle_G. \tag{24}$$

C. MD and Boltzmann evolution comparison

To show that the kernel, K, contains the information of the thermalization dynamics, we use it to evolve $h(v, 0) = \delta(v)$ according Eq. (11) and compare the evolved distribution to that of the MD simulation. We tested several values of the evolution time t_f and different values for the system parameters. When N is big and ρ is small, the Boltzmann and the MD evolved distributions are in agreement as shown in Fig. 5. This demonstrates that the collision kernel, K, describes the thermalization process in the low-density limit. For the comparison presented here, we use system parameters $N = 161$, $R = 51\,200\,\mu\text{m}$, $l_0 = 1\,\mu\text{m}$, $n = 6$, $\epsilon = 1\,\text{eV}$, $kT = 100\,\text{meV}$, $m = m_e$, and $t_f = 12\,800\,\text{ns} = 1.6 \times 10^{-4}/\Gamma$, where Γ is computed from Eq. (18) using $\rho = (N-1)/(2\pi R) \approx 0.5\,\text{mm}^{-1}$.

For smaller N or bigger ρ, we get a slight disagreement between the two methods. Four-body collisions are significant when ρ becomes large, which is not accounted for in the collision kernel, K. Moreover, at fixed ρ, the MD simulations require large N for convergence because the perturbation, h, has a large effect on the thermal particles for smaller N.

Equipped with the kernel, we can evolve the system for longer times using the Boltzmann Eq. (11). First, we calculated the kernel for a slow moving special particle $u' = -0.25$ and found the kernel G is approximately translation invariant as later demonstrated in Fig. 8. That is,

$$G_{0\to u} \approx G_{u'\to u'+u}, \tag{25}$$

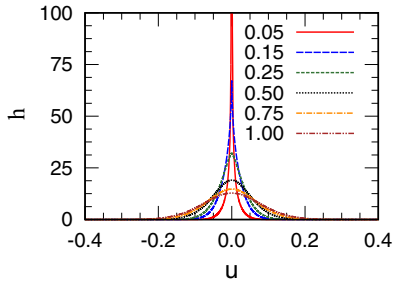

FIG. 6. Evolution of the perturbation, $h(u,t)$, at different times and approach toward equilibrium. Gas parameters are $N = 161$, $n = 6$, $R = 51\,200\,\mu\text{m}$, $\epsilon = 1\,\text{eV}$ and $kT = 100\,\text{meV}$, m is the mass of the electron. Figure legends represent the time for the distribution in fraction of $0.01/\Gamma$, where Γ is computed from Eq. (18). There are two stages for the peak of the perturbation: non-Gaussian cusp and smooth Gaussian.

for $|u'| \ll 1$. Therefore, the only information needed to propagate small velocities to good accuracy is $G_{0\to u}$. In this limit, the change in h during successive time steps in Eq. (10) becomes a repeated convolution integral.

Figure 6 shows the evolution of the δ perturbation over a timescale $t_f = 0.01/\Gamma$ as computed from the Boltzmann Eq. (10). The system's parameters are $N = 161$, $R = 51\,200\,\mu\text{m}$, $n = 6$, $\epsilon = 1\,\text{eV}$, $kT = 100\,\text{meV}$, $m = m_e$, where Γ is computed from Eq. (18) and $\rho = (N-1)/(2\pi R)$. At early times $t_f\Gamma < 1 \times 10^{-3}$, h has a cusp maximum which resembles that of G. That is because the change in h is approximately proportional to G as in Eq. (9) when G is highly localized. At later times $t_f\Gamma \sim 1 \times 10^{-2}$, the cusp flattens out as repeated convolutions relax the population to a Gaussian distribution, which subsequently spreads at a steady rate during the range of time considered. The relaxation to a Gaussian is a consequence of the repeated convolution and the central-limit theorem [20].

The spread of the perturbation in Fig. 6 indicates that its variance (which is proportional to the energy) is growing with time which is shown in Fig. 7. The linear evolution of the perturbation's energy in the time range considered indicates the thermalization rate defined through Eq. (8) is approximately constant with time and does not depend strongly on the shape of perturbation. It also suggests modeling the thermalization process as a random walk of the velocity u' of the special particle. The standard deviation of h is proportional to $\sqrt{t}$, just like the standard deviation of displacement in a random

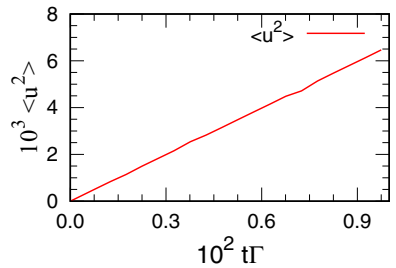

FIG. 7. The variance $\langle u^2 \rangle_h$ of the perturbation growing linearly with time. The evolution of h itself is plotted in Fig. 6.

TABLE I. Rate constants a_n and fitting parameters for different potential powers n. The uncertainty in α, β, and σ is ± 0.001.

n	a_n	α	β	σ	$\lvert u_{1f,\max}\rvert$
2	0	0.000			1×10^{-7}
4	3.49×10^{-4}	0.237	1.182	0.022	2.69×10^{-2}
6	2.58×10^{-4}	0.182	1.117	0.027	3.06×10^{-2}
8	1.62×10^{-4}	0.148	1.076	0.025	2.76×10^{-2}
10	1.02×10^{-4}	0.129	1.046	0.021	2.37×10^{-2}
12	6.55×10^{-5}	0.115	1.023	0.018	2.04×10^{-2}

walk is proportional to the square root of the number of steps taken.

Each three-body collision with the thermal particles gives the special velocity a random kick leading to a random walk in velocity space. Using the order of magnitude of a_n in Tab. I, it takes $\sim 1/a_n \sim 10^4$ kicks to thermalize, i.e., the variance $\langle u^2 \rangle$ approaching 1. The kick magnitude is $\sim\sqrt{a_n} \sim 0.01$, which is of the order of magnitude of the strongest kick in a three-body collision (as explained in Sec. IV E).

D. G for a moving special particle $u' \neq 0$

In this section, we demonstrate how other velocity perturbations $u' \neq 0$ (moving special particles) scatter within the bath due to three-body collisions. Since the kernel is proportional to the transition rates, Fig. 8 shows that a perturbation near the tail of the Maxwell-Boltzmann distribution at $u' = -3.0$ scatters to neighboring velocities more rapidly than from $u' = 0$. However, scattering from small velocities such as $u' = -0.25$ is almost identical to $u' = 0$.

For several values of u', the initial rate of change of the mean scaled velocity $d\langle u \rangle/dt$ and the variance $d\langle (u-u')^2 \rangle/dt$ are calculated as in Eq. (23) and are shown in Fig. 9. In particular, negative velocity perturbations have a positive initial rate of change of the average, which is a drag effect that slows down the special velocity. Also, we note that the initial rate of change of the variance only changes by a factor of ~ 2. This indicates that the definition of Γ in Eq. (8) leads to a reasonable estimate of the time required for thermalization (i.e., Γ does not strongly depend on u').

From the $\langle (\Delta u)^2 \rangle$ curve, bigger velocity perturbations transition faster to neighboring velocities. This is an indication

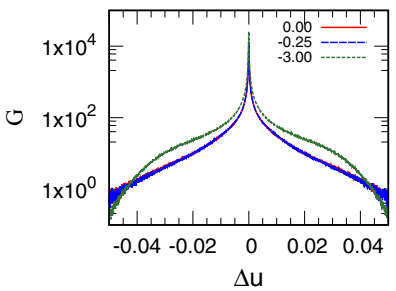

FIG. 8. Kernel G for different special velocities. A perturbation at the tail scatters faster than a perturbation at the center. The $u' = -3.0$ curve is slightly skewed to the right as shown in the first moment $\langle u \rangle$ in Fig. 9. The x axis here is $\Delta u = u - u'$.

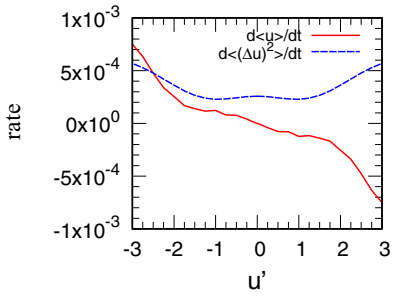

FIG. 9. Initial rate of change (scaled by $\rho^2 l v_{\rm th}$) of the first moment $\langle u \rangle$ and the variance $\langle (u-u')^2 \rangle$ for perturbations localized at different velocities. The calculations were done for negative u', but were reflected to extend over positive u' for clarity. The small fluctuations in the curves are due to statistical noise.

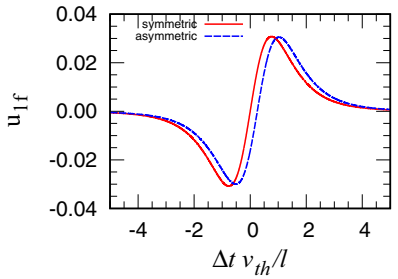

FIG. 11. Scaled kick u_{1f} as a function of the scaled delay $(\Delta t v_{\rm th}/l)$ between launches. The symmetric case is for $u_{2i} = 1$ and $u_{3i} = -1$, while the asymmetric case is for $u_{2i} = 1.1$ and $u_{3i} = -0.9$. The curve for the asymmetric case was shifted horizontally for clarity. Both curves have long tails and peak at $u_{1f,\rm max} \sim 0.03$.

of detailed balance [21] which we numerically checked for pairs of velocity states. For example, the bins at $u = -3.00$ and $u = -2.96$ exchange populations at rates compatible with the steady state Maxwell-Boltzmann distribution. That is, for $n = 6$ we numerically found that

$$\frac{G_{-3.00\to-2.96}}{G_{-2.96\to-3.00}} = 1.12 \pm 0.04, \tag{26}$$

while the ratio between the Maxwell-Boltzmann populations at the corresponding bins is $e^{-2.96^2/2}/e^{-3.00^2/2} = 1.13$.

E. Dependence of G on the potential power n

Figure 10 shows how the kernel compares for different powers n in the inverse power potential, Eq. (1). The scaled kernel is generally smaller for bigger n, indicating that the special particle scatters more slowly when the potential is steeper. Particularly, in the limit $n \to \infty$, the potential in Eq. (1) approaches hard walls at $|d| = l_0$, and the binary collision is an instantaneous velocity swap of two particles of size $2l_0$. In such a limit, a ternary coincidence [Eq. (21)] necessary for thermalization is impossible. This is reflected in the decrease of a_n with increasing n, where the values of a_n computed using Eq. (24) are shown in Table I.

To understand why the kernel has its shape and why different values of n produce different shapes, we fitted the kernel guided by the details of the MC simulation. In Fig. 8, the kernel $G_{-3.0\to-3.0+\Delta u}$ near $\Delta u = 0$ decreases rapidly with

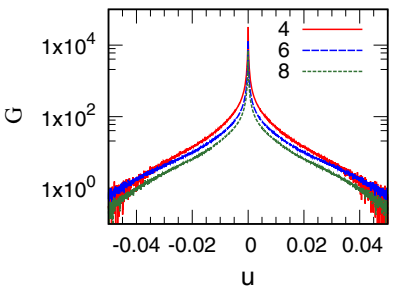

FIG. 10. The collision kernel $G_{0\to u}$ for different potential power n values. $G_{0\to u}$ is generally bigger for smaller n for the range of u shown.

increasing $|\Delta u|$, and decreases more rapidly for $|\Delta u| >\sim 0.03$. To capture both of these features, G can be fitted to a Gaussian modulated power law:

$$g(u) = \frac{\alpha}{|u|^\beta} e^{-u^2/2\sigma^2}, \tag{27}$$

as shown in Fig. 4 for $n = 6$. The parameters α, β, and σ are shown for several values of n in Table I. The α parameter is proportional to the over all scattering rate, and the power β measures how fast the kernel drops with increasing $|u|$ near $u = 0$ as in Fig. 4. We observe that both α and β decrease as n increases (i.e., when the potential is becoming steeper and approaching hard walls).

The choice of such fitting function can be explained by inspecting monoenergetic collisions in which the incoming energies are fixed as opposed to having a continuous "thermal" distribution. Figure 11 shows the effect on the special particle starting from zero velocity in two launching cases: a symmetric case $v_2 = v_{\rm th}$, $v_3 = -v_{\rm th}$, and an asymmetric case $v_2 = 1.1 v_{\rm th}$, $v_3 = -0.9 v_{\rm th}$. The final kick the special particle receives, u_{1f}, is plotted against the delay Δt between launching particles 2 and 3. Both curves look similar with long tails for $|\Delta t| \gtrsim 3l/v_{\rm th}$. The long tails happen because a large delay results in a tiny momentum transfer to the special particle. They are responsible for the fast drop of the kernel $G_{0\to u}$ around $u = 0$, which is captured in the power-law term of the fitting function g. Moreover, both curves peak at a maximum momentum transfer $u_{1f,\rm max} \sim 0.03$. The Gaussian modulation term in Eq. (27) is a way to average over the distribution of the launched particles from the thermal environment. Its width σ is not of order 1 but rather reflects the value of the fractional momentum transfer $u_{1f,\rm max}$. In particular, σ correlates with $|u_{1f,\rm max}|$; they both peak at $n = 6$ and drop monotonically away from $n = 6$ as shown in Table I.

For $n = 2$, $|u_{1f,\rm max}|$ was found to be $\approx 1 \times 10^{-7}$ which is not different from 0 within errors resulting from the numerical solution of the equations of motion, Eq. (19). In fact, for the inverse square power potential it was shown that the equations of motion are integrable and the potential is, surprisingly, isospectral (momenta only trivially swap) [14]. That means that a system with such pairwise interaction can only thermalize through four or higher body collisions.

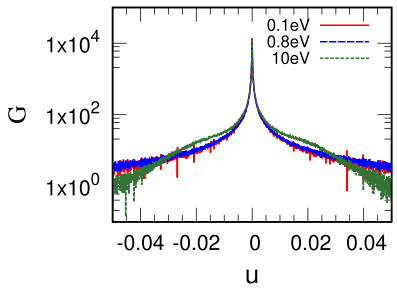

FIG. 12. Scaled collision kernel for different kT with $\epsilon = 1eV$ and other parameters from Sec. IV B. The small temperature curves overlap, but the high temperature curve deviates indicating the lack of scaling symmetry.

F. Broken scaling in Lennard-Jones potential

In contrast with the inverse power-law potential in Eq. (1), the Lennard-Jones potential is

$$U_{LJ}(d) = \epsilon\left[\left(\frac{l_0}{d}\right)^{12} - \left(\frac{l_0}{d}\right)^{6}\right]. \tag{28}$$

This potential is different from the inverse power potential in important ways. First, it is attractive at long distance. Moreover, there is possibility of three-body recombination. Most importantly, the scaling of the inverse power potential is lost in the Lennard-Jones potential. That is, we cannot fix the potential energy scale to kT as we did in Eq. (13).

Figure 12 shows $G_{0\to u}$ for the Lennard-Jones potential for three different temperatures $kT = 0.1,\ 0.8$, and 10 eV. In all cases, the potential energy scale $\epsilon = 1$ eV. When the kinetic energy (kT) is small compared to the potential energy, the scaled $G_{0\to u}$ is almost the same for different temperatures as seen in the 0.1 and 0.8 eV curves. When the kinetic energy is larger, $G_{0\to u}$ has a significantly different shape as seen in the 10 eV curve. This shows the universal scaling (compare to Fig. 4) remains approximate at low T but is lost at high T. The simulation parameters are the same as those used for Fig. 4. The G kernel here is still scaled by l defined through Eq. (14) with $n = 6$. For $kT = 100$ meV, the dimensionless thermalization rate a_n is found to be 3.00×10^{-4}, which is bigger than that of the power-law potential with $n = 6$ by 16%. Thus, the Lennard-Jones potential gives qualitatively similar thermalization rates to the inverse power potential even with the differences noted above.

It is interesting to compare the rate of three-body recombination to the rate of thermalization for 1D and 3D gases. In the present 1D gas, both processes involve three particles, and their rates scale like ρ^2. In dilute 3D gases, thermalization is a two-body process (with rate $\propto \rho$) and happens at a much faster rate than three-body recombination. Moreover, for fixed ρ in our 1D gas, we find that the ratio of three-body recombination rate to thermalization rate drops rapidly with increasing T. This could be explained by noting that at low T, a pair of particles approaching each other from far distance have small positive relative energy. If a third particle interacts with the pair, there is a high chance that the energy of the pair transfers to the third particle, leaving the pair in a bound state with negative relative energy. At high T, the chances of the third particle taking away enough energy to switch the sign of the energy of the pair is small.

V. CONCLUSION

We have studied the rates of classical three-body thermalization in dilute one-dimensional gases with inverse power-law interaction with $n > 2$ for various system parameters. Through MD simulations of the N-body gas and MC simulations of the three-body scattering kernel, we showed that the gas relaxes with a rate proportional to $\rho^2\sqrt{\frac{kT}{m}}l_0(\frac{\epsilon}{kT})^{\frac{1}{n}}$. The scaling of the thermalization rate in terms of T is exact for the inverse power potential, but only approximate at low T for the Lennard-Jones potential.

Classical three-body thermalization in 1D is significantly slow (compared to higher-dimensional gases) not only due to the ρ^2 scaling, but also the smallness of the proportionality constant, which comes from the weak redistribution of energy in each collision. The implication is that dilute 1D gases preserve their out-of-equilibrium states for a relatively long time. For example, a 1D Nitrogen atom gas with $\rho = 1$ atom/10 μm at $T = 10$ K interacting under the Nitrogen-Nitrogen Lennard-Jones potential takes around 10s to thermalize according to Eq. (23) and parameters found in Ref. [22].

By rewriting the equations of motion in a dimensionless way, we provided arguments for the scaling of both MD and MC simulations, which we verified numerically. Moreover, we have shown that the Boltzmann equation using a three-body collision kernel is sufficient to reproduce the evolution of low-density N-body gas calculable from MD simulations. Additionally, the collision kernel behaves like a power law for small momentum transfer. For bigger momentum transfer, it is modulated by a Gaussian with width of order of the maximum momentum transfer during a monoenergetic collision. Finally, the collision kernel provided us with an understanding of how the overall rates and the statistical details of three-body scattering depend on the potential power n.

Data for the figures used in this publication are available from the Purdue University Research Repository [23].

ACKNOWLEDGMENT

This work was supported by the U.S. Department of Energy, Office of Science, Basic Energy Sciences, under Award No. DE-SC0012193.

APPENDIX A: MOLECULAR DYNAMICS SIMULATION

In this Appendix, we provide details and analysis of the MD simulations. To simulate the gas of N particles in Fig. 1, the initial velocities are chosen as per Eq. (5), whereas the initial locations are chosen randomly according to a relative potential energy Boltzmann factor. We evolve the system from time $t_i = 0$ to time t_f according to Eq. (12) using Runge-Kutta methods with adaptive time step [24]. At t_f, we subtract the background thermal distribution as per Eq. (5) to single out the perturbation $h(v, t_f)$. We average over many trajectories

with different initial conditions and average over a window of time around t_f to reduce the statistical noise.

The number of terms in the force calculation in Eq. (12) scales like N^2 for a single time step, which makes it difficult to simulate more than 30 particles. To decrease the computational time, we utilize that the inverse power potential in Eq. (1) is relatively "short range" for $n \geqslant 2$ and small density ρ. In this regime, particles are only interacting significantly with their close neighbors, while the interaction with further particles can be ignored. This allows us to do nearest neighbors calculations for the force, which results in a time complexity that scales like N. This approximation is similar to truncating the potential at certain particle separation as usually used in the MD simulation for the Lennard-Jones potentials [25]. The neighbors are selected by ordering the particles according to their initial locations. For three nearest neighbors, for example, particle number 5 experiences a force from particles numbered 2–4 and 6–8. Since the potential is infinitely repulsive at short distance, the particles cannot pass through each other and the particle order is fixed. We checked that the results converged for three nearest neighbors which was used for all MD simulations in this paper. Using this method, we could simulate more than 160 particles.

To ensure that three-body collisions are the largest effect, we choose a small density $\rho = (N-1)/2\pi R$. We verify the ρ^2 scaling by simulating a density ρ for time t_f and comparing the final h to that of another simulation with $\rho/2$ (by doubling R for a given N) for time $4t_f$. The results converge for densities near ($\rho l \sim 1 \times 10^{-3}$). From analysis of the Runge-Kutta with adaptive time step algorithm, the related best-case time complexity scales like $1/\rho$.

Once we fix the convergence density, we double N and R in steps to obtain thermodynamic convergence. The results converge for particle number near $N = 160$. Once we fix the convergence particle number, we run the simulation for a longer time to get appreciable evolution of h. All these considerations combined render the MD simulations computationally expensive, and we chose to limit the simulation time to t_f of the order $1 \times 10^{-4}/\Gamma$, where Γ is from Eq. (18).

APPENDIX B: BOLTZMANN EQUATION

In the kinetic theory of gases, the state of a gas in 1D is described by the aggregate one-particle distribution in coordinate-velocity space $f(x, v, t)\,dxdv$. The evolution of such distribution is described by the Boltzmann equation [18]:

$$\frac{\partial f}{\partial t} + v\frac{\partial f}{\partial x} + \frac{f}{m}\frac{\partial f}{\partial v} = \left(\frac{\partial f}{\partial t}\right)_c, \tag{B1}$$

where f is the external force and m is the mass of the particle. For an isolated system with uniform density ρ, which we assume in our work, the velocity and space derivative terms drop out. In this case, the only way to change f is through interparticle interactions dictated by the collision term on the right-hand side. (Henceforth, we use f to represent the distribution in velocity only. The one-particle velocity-space distribution is ρf, where ρ is the number density.) The collision term is modeled and computed in the MC simulation in Appendix C.

APPENDIX C: MONTE CARLO SIMULATION

In this Appendix, we provide the relevant distributions and steps of the Monte Carlo Algorithm for generating the discrete version of $K_{v'\to v}$. First, we treat the case of an initially stationary special particle, $v' = 0$. The one-particle phase space thermal distribution is given by ρf_0 where f_0 is the equilibrium velocity distribution in Eq. (4). At $x = L/2$, particles are entering the observation region with negative velocity. The rate of entry is equal to the probability current (flux) $\rho f_0|v|$ integrated from $v = -\infty$ to 0. We get the same rate from the left. So overall we get a rate of

$$r = \int_{-\infty}^{+\infty} \rho f_0(v)|v|\,dv = \rho v_{\rm th}\sqrt{\frac{2}{\pi}}, \tag{C1}$$

and a velocity distribution of the launched particles

$$P_{\rm launch}(v) = \rho f_0(v)|v|/r, \tag{C2}$$

which is the probability that v lies between $v - dv/2$ and $v + dv/2$ per dv (normalized so the integral over all v is 1).

To treat the case $v' \neq 0$, we go to the reference frame moving with v'. The distribution in that frame is $\rho f_0(v + v')$; therefore, the launching rate is generally

$$\begin{aligned} r &= \int_{-\infty}^{\infty} \rho f_0(v + v')|v|\,dv \\ &= \frac{\rho v_{\rm th}}{\sqrt{2\pi}} \int_{-\infty}^{\infty} e^{-(u+u')^2}|u|\,du \\ &= \frac{\rho v_{\rm th}}{\sqrt{2\pi}}\left[2e^{\frac{-u'^2}{2}} + \sqrt{2\pi}u'\,\mathrm{erf}\left(\frac{u'}{\sqrt{2}}\right)\right], \end{aligned} \tag{C3}$$

where erf is an error function. The general launch distribution for velocity is

$$P_{\rm launch}(v) = \rho f_0(v + v')|v|/r. \tag{C4}$$

The rate r determines the probability distribution for a delay time between the launching of particles 2 and 3:

$$P_{\rm delay}(\Delta t) = re^{-r\Delta t}. \tag{C5}$$

Using these distributions, we implement the MC simulation as follows: (1) At time $t = 0$, particle 1 is initialized at $x = 0$ with $v_1 = 0$. (2) Particle 2 is initialized with a random velocity v_2 picked from the distribution $P_{\rm launch}(v)$ in Eq. (C4) at $x = \pm L/2$ depending on the sign of v_2. (3) Particle 3 is initialized with a random velocity v_3 picked from the distribution $P_{\rm launch}(v)$ at $x = \pm L/2$ depending on the sign of v_3, with a random time delay Δt chosen according to $P_{\rm delay}(\Delta t)$ in Eq. (C5). (4) The three initial velocities v_1, v_2, and v_3 are added to the appropriate bins (histogram) of the discretized approximation of K, Eq. (11), with a value of -1 because these velocities are destroyed through the collision. (5) Using Runge-Kutta methods, the particles are propagated until they collide and separate appreciably. (6) The final velocities w_1, w_2, and w_3 are added to the histogram with a $+1$ because these velocities are created. (7) Steps 1–6 are repeated for a number of trajectories $N_{\rm traj}$ until the statistical noise decreases to a sufficient level. (8) The histogram is divided by $N_{\rm traj} t_{\rm avg}\Delta v$ where $t_{\rm avg}$ is the inverse of the rate r. This discretized approximation converges to $K_{v'\to v'+v}$ in the limit $N_{\rm traj} \to \infty$ and $\Delta v \to 0$.

This prescription is a Monte Carlo evaluation of the scattering kernal where our δ-perturbative model of the collision term can be read from Eq. (10) as

$$\left(\frac{\partial h}{\partial t}\right)_c = \int_{-\infty}^{\infty} K_{v'\to v} h(v', t)\, dv', \tag{C6}$$

where K is computed from the MC simulation. For $v' = 0$,

$$K_{0\to v} = \iiint dv_2 dv_3 d\Delta t \frac{\rho f_0(v_2)|v_2|}{r} \frac{\rho f_0(v_3)|v_3|}{r} \times r e^{-r\Delta t} \times r[-\delta(v) - \delta(v_2 - v) - \delta(v_3 - v) + \delta(w_1 - v) + \delta(w_2 - v) + \delta(w_3 - v)], \tag{C7}$$

where w_1, w_2, w_3 are the outgoing velocities of the collision and are functions of the incoming velocities v_2, v_3 and the time delay Δt. r is the rate of launching in Eq. (C1), and f_0 is the Maxwell distribution in Eq. (4). The first three terms in the integrand are the normalized distributions (integral over the respective domain being 1) of v_2, v_3, and Δt. The last term ($r\times$the square bracket) is the rate of destruction subtracted from the rate of creation of velocity v. For special velocity $v' \neq 0$, we get a similar integral expression but with the velocity arguments shifted as in Eq. (C4) and r defined in Eq. (C3).

Our collision term is comparable to that in Ref. [10] which is derived for two-body collisions in 3D using the differential cross-section. It is also comparable to that in Ref. [15], which handles three-body collisions in 1D but assumes constant transition rates for all v_1, v_2, $v_3 \to w_1, w_2, w_3$ interactions compatible with energy and momentum conservation. The collision term in Ref. [15] yields an analytically solvable Boltzmann Equation, but is not derivable from an interparticle interaction.

[1] J. Christen, M. Grundmann, E. Kapon, E. Colas, D. Hwang, and D. Bimberg, Ultrafast carrier capture and long recombination lifetimes in GaAs quantum wires grown on nonplanar substrates, Appl. Phys. Lett. **61**, 67 (1992).

[2] K. H. Baloch, N. Voskanian, M. Bronsgeest, and J. Cumings, Remote Joule heating by a carbon nanotube, Nat. Nanotechnol. **7**, 316 (2012).

[3] T. M. O'Neil and P. G. Hjorth, Collisional dynamics of a strongly magnetized pure electron plasma, Phys. Fluids **28**, 3241 (1985).

[4] S. Erne, R. Bücker, T. Gasenzer, J. Berges, and J. Schmiedmayer, Universal dynamics in an isolated one-dimensional Bose gas far from equilibrium, Nature (London) **563**, 225 (2018).

[5] M. Moško and V. Cambel, Thermalization of a one-dimensional electron gas by many-body Coulomb scattering: Molecular-dynamics model for quantum wires, Phys. Rev. B **50**, 8864 (1994).

[6] F. Haldane, "Luttinger liquid theory" of one-dimensional quantum fluids. I. Properties of the Luttinger model and their extension to the general 1D interacting spinless Fermi gas, J. Phys. C: Solid State Phys. **14**, 2585 (1981).

[7] R. Livi, Anomalous transport in low-dimensional systems: A pedagogical overview, Phys. A: Stat. Mech. Appl. **631**, 127779 (2023).

[8] L. Rota, F. Rossi, S. M. Goodnick, P. Lugli, E. Molinari, and W. Porod, Reduced carrier cooling and thermalization in semiconductor quantum wires, Phys. Rev. B **47**, 1632 (1993).

[9] M. Panfil, S. Gopalakrishnan, and R. M. Konik, Thermalization of interacting quasi-one-dimensional systems, Phys. Rev. Lett. **130**, 030401 (2023).

[10] G. Uhlenbeck, G. Ford, and E. Montroll, *Lectures in Statistical Mechanics: By G.E. Uhlenbeck and G.W. Ford; with an Appendix on Quantum Statistics of Interacting Particles by E.W. Montroll*, Lectures in applied mathematics (American Mathematical Society, Providence, RI, 1963).

[11] L. D. Landau and Lifshitz, *Statistical Physics* (Butterworth-Heinemann, Oxford, UK, 1981).

[12] J.-B. Fouvry, P.-H. Chavanis, and C. Pichon, Kinetic theory of one-dimensional homogeneous long-range interacting systems with an arbitrary potential of interaction, Phys. Rev. E **102**, 052110 (2020).

[13] A. J. Maciejewski and M. Przybylska, Non-integrability of the three-body problem, Celest. Mech. Dyn. Astr. **110**, 17 (2011).

[14] F. Calogero and C. Marchioro, Exact solution of a one-dimensional three-body scattering problem with two-body and/or three-body inverse-square potentials, J. Math. Phys. **15**, 1425 (1974).

[15] S. K. Ma, One-dimensional Boltzmann equation with a three-body collision term, J. Stat. Phys. **31**, 107 (1983).

[16] J.-B. Fouvry, B. Bar-Or, and P.-H. Chavanis, Kinetic theory of one-dimensional homogeneous long-range interacting systems sourced by $1/N^2$ effects, Phys. Rev. E **100**, 052142 (2019).

[17] D. P. Kroese, T. Taimre, and Z. I. Botev, *Handbook of Monte Carlo Methods* (John Wiley & Sons, New York, NY, 2013).

[18] R. Zwanzig, *Nonequilibrium Statistical Mechanics* (Oxford University Press, Oxford, UK, 2009).

[19] D. J Evans and G. P Morriss, *Statistical Mechanics of Nonequilbrium Liquids* (ANU Press, Canberra, 2007).

[20] A. Klenke, *Probability Theory: A Comprehensive Course* (Springer Science & Business Media, Cham, 2013).

[21] A. Gorban, Detailed balance in micro- and macrokinetics and micro-distinguishability of macro-processes, Results Phys. **4**, 142 (2014).

[22] B. Mamedov and E. Somuncu, Analytical treatment of second virial coefficient over Lennard-Jones ($2n - n$) potential and its application to molecular systems, J. Mol. Struct. **1068**, 164 (2014).

[23] Data for: Simulations of classical three-body thermalization in one dimension, https://doi.org/10.4231/7ME4-BG45 (2024).

[24] W. H. Press, *Numerical Recipes: The Art of Scientific Computing*, 3rd ed. (Cambridge University Press, Cambridge, UK, 2007).

[25] N. Giordano, *Computational Physics*, 2nd ed. (Dorling Kindersley, London, UK, 2012).